View metadata, citation and similar papers at core.ac.uk

brought to you by CORE

provided by Explore Bristol Research

Scarth, C., Sartor, P. N., Cooper, J. E., Weaver, P. M., & Silva, G. H. C. (2015). Robust aeroelastic design of composite plate wings. In 17th AIAA Non-Deterministic Approaches Conference. [AIAA 2015-0918] American Institute of Aeronautics and Astronautics Inc.. 10.2514/6.2015-0918

Peer reviewed version

Link to published version (if available):
10.2514/6.2015-0918

Link to publication record in Explore Bristol Research
PDF-document

University of Bristol - Explore Bristol Research

General rights

This document is made available in accordance with publisher policies. Please cite only the published version using the reference above. Full terms of use are available:
http://www.bristol.ac.uk/pure/about/ebr-terms.html

Take down policy

Explore Bristol Research is a digital archive and the intention is that deposited content should not be removed. However, if you believe that this version of the work breaches copyright law please contact open-access@bristol.ac.uk and include the following information in your message:

• Your contact details
• Bibliographic details for the item, including a URL
• An outline of the nature of the complaint

On receipt of your message the Open Access Team will immediately investigate your claim, make an initial judgement of the validity of the claim and, where appropriate, withdraw the item in question from public view.

Robust Aeroelastic Design of Composite Plate Wings

Carl Scarth[1], Pia N. Sartor[2], Jonathan E. Cooper[3] and Paul M. Weaver[4]
Department of Aerospace Engineering, University of Bristol, Bristol, BS81TR, UK

and

Gustavo H.C. Silva[5]
Embraer S.A., São José dos Campos, São Paulo, 12227-901, Brazil

An approach is presented for the robust stacking sequence design of composite plate wings with uncertain ply orientations. An aeroelastic model is constructed using the Rayleigh-Ritz technique coupled with modified strip theory aerodynamics. Gaussian processes are used as emulators for the aeroelastic instability speed in order to efficiently quantify the effects of uncertainty. The critical instability speed is discontinuous as a result of the different potential instability mechanisms, therefore multiple Gaussian processes are fitted to ensure computational efficiency. An order of two magnitude reduction in model runs is achieved for the majority of examples, and an order of magnitude reduction is achieved when a switch between flutter modes occurs. The emulators are used to estimate the probability that instability occurs at a given design speed, which is minimized using a genetic algorithm. Results are compared to deterministic optima for maximal instability speed. Two lay-up strategies are undertaken, a first in which ply orientations are limited to 0°, ±45° and 90°, and a second in which values of ±30° and ±60° may also be taken. Improvements in reliability of at least 85% are achieved. The inclusion of ±30° and ±60° plies enables a 1.7% increase in the nominal instability speed, and an increase in reliability of at least 59%.

Nomenclature

a_w	=	Lift-curve slope
A	=	Inertia matrix, training data covariance
B	=	Aerodynamic damping matrix
c	=	Chord length, covariance function
c^*	=	Emulator covariance
C	=	Aerodynamic stiffness matrix
e	=	Eccentricity of flexural axis from quarter-chord
D	=	Out-of-plane laminate stiffness matrix
E	=	Stiffness matrix, expected value operator
E_{ij}	=	Young's modulus in the ij direction, $i = j = 1, 2$
G_{12}	=	Shear modulus
L	=	Applied lift
m^*	=	Emulator mean
$\boldsymbol{M}, M$	=	Bending moment resultant vector, applied pitching moment
$M_{\dot{\theta}}$	=	Unsteady aerodynamic derivative
n	=	Number of training data points, number of test points
$\boldsymbol{q}$	=	Generalized coordinates vector
s	=	Semi-span

[1] PhD Student.
[2] Lecturer in Aerospace Engineering.
[3] RAEng Airbus Sir George White Professor of Aerospace Engineering. AFAIAA
[4] Professor in Lightweight Structures.
[5] Technology Development Engineer.

t, $\boldsymbol{t}$ = Laminate thickness, test data covariance
T = Kinetic energy
U = Strain energy
U_i = Material invariants, i = 1-5
V = Air speed
V_{crit}, V_{des} = Critical aeroelastic instability speed, design aeroelastic instability speed
w = Out-of-plane deformation
W = Work done
x, y, z = Cartesian coordinate system
$\boldsymbol{x}$ = Model input vector
y = Model output, design variable
y_f = Flexural axis location
θ = Ply orientation, elastic twist
$\boldsymbol{\kappa}$ = Curvature vector
λ_i = i^{th} eigenvalue of the equation of motion
ρ = Density
ρ_a = Air density
ν_{12} = Poisson's ratio
ξ_i = Out-of-plane lamination parameters, i = 9-12
$\boldsymbol{h}$, $\boldsymbol{\beta}$, σ^2, B = Emulator hyperparameters

I. Introduction

Composite materials are being used to an increasing degree in aerospace structures due to a number of useful attributes including high specific strength and stiffness, and anisotropic behavior which may be exploited to tailor properties. A large amount of work has been undertaken since the 1980s in the field of aeroelastic tailoring[1-6]; this has sought to exploit anisotropy through selection of composite stacking sequences which achieve minimum-weight designs for aeroelastic design cases while adhering to loading and aerodynamic design constraints. Example applications have included divergence[1] and flutter[2-4], as well as gust and manoeuvre loads[5,6].

While models can represent aeroelastic behavior to a high degree of accuracy, in reality all processes are subject to variability. Composite materials require complex manufacturing processes which can introduce uncertainty from a number of sources including material non-homogeneity, fibre misalignment, waviness and wrinkling[7], and defects resulting from dropped plies[8]. There is a need[9] for aeroelastic models which incorporate parametric uncertainties such as these, in order to quantify the effect of this uncertainty and to identify robust designs which are insensitive to small variations in properties.

Uncertainty in composite structures[10,11,12] and aeroelastic stability[9,13,14] have been investigated using a variety of techniques. Monte Carlo Simulation (MCS) and the perturbation method were used[10] to model buckling and supersonic flutter of a composite plate with uncertain ply orientations, and to model flutter of a composite beam with uncertain ply orientations and moduli[11]. MCS is the most straightforward uncertainty quantification technique, however, prohibitively large computational effort is required to give meaningful results. The perturbation method models uncertainties as Taylor series expansions of small perturbations from the mean, though cannot be used to obtain the full output distribution. Polynomial Chaos Expansion (PCE) has been used to model uncertainty in a number of models, such as a pitch and plunge aerofoil model with uncertain spring stiffness coefficients[9] a composite plate with uncertain ply orientions[12], and a flat plate subject to uncertain aerodynamic load[13]. Stochastic Collocation has been used for numerous applications, including the bifurcation analysis of a pitching aerofoil with uncertain nonlinear stiffness, natural frequency and equilibrium pitch angle[14]. The latter two techniques enable efficient uncertainty quantification through fitting polynomial surrogate models; orthogonal polynomials from the Askey scheme are used for Polynomial Chaos Expansion[15] and Lagrange polynomials for Stochastic Collocation[16]. Both techniques are limited by the 'curse of dimensionality'[17], wherein the number of model runs required to fit the surrogate increases dramatically with input dimension.

A Gaussian process can be thought of as a Gaussian distribution over functions[18], and can be used as an emulator, a form of surrogate model. Gaussian process emulators can be fitted to relatively high dimension models with relatively little computational effort, and have been used for a number of applications including experiment design[19], uncertainty quantification[20] and sensitivity analysis[21].

A number of approaches can be taken to determine optimal designs which are insensitive to uncertainty. Reliability is a measure of the probability of survival within the design envelope, and is often used as either an objective or

constraint in reliability-based design optimization (RBDO). The reliability index is often used to estimate reliability, and is given by the distance between the most probable point of failure and the mean of the input parameters when transformed into standard normal space[22]. Techniques such as the First Order Reliability Method (FORM) and Second Order Reliability Method (SORM) can be used to predict the reliability index by approximating the limit state function which defines failure of a given design, by using first and second order Taylor series expansions respectively. For example, FORM has been used to find the ply orientation and wing twist which maximises the probability of achieving a specified lift-to-drag ratio in a two-ply composite plate wing with uncertain angle of attack and thickness[23]. Alternatively, robustness can be defined as the extent to which perturturbations can be made from nominal parameter values without violating hard inequality constraints. This approach has been applied to the optimal placement of a moveable mass in order to avoid flutter of an aerofoil with uncertain bending and torsional stiffness, and aerodynamic loading[24]. A robust design optimization (RDO) seeks to trade off sensitivity to uncertainty against mean performance in a multi-objective optimization[25].

Surrogate modeling techniques can be used to reduce the computational effort required for each of the above approaches. For example, PCE has been used to maximize lift-to-drag ratio of an aerofoil while minimizing the variance due to uncertainty in leading-edge thickness[26]. Likewise, Polynomial Chaos has been used to approximate and minimize the probability of aeroelastic instability in the stacking sequence optimization of six-ply composite plate wings with uncertain ply orientations, moduli and laminate thickness[27].

This paper is a preliminary investigation into the use of Gaussian process surrogate modeling techniques for the efficient robust design of composite plate wings with uncertainty in ply orientation. A composite wing is idealised as a flat rectangular plate. A structural model is constructed using the Rayleigh Ritz technique and used to assess the stability of the wings. Gaussian processes are fitted to the model and used to emulate the aeroelastic instability speed. The lowest instability speed is discontinuous with respect to model inputs, as changing the composite layup can lead to switches between different instability mechanisms, for example from divergence to flutter. As such it is necessary to fit multiple emulators to the different instability speeds. Probability Density Functions (PDFs) are estimated for a number of example composite laminates using the emulators, and compared to PDFs determined using the model itself. Finally, a genetic algorithm is used to determine optimal composite layups for deterministic and robust objectives using different layup strategies. Baseline deterministic optima for maximal instability speed are obtained firstly by fixing ply orientations to their nominal values. Uncertainty is subsequently introduced to the ply orientations, and then probability of failure is estimated using the emulator, and minimized to find a robust design. Reliability of the deterministic and robust optima are compared alongside a number of useful statistics.

II. Model Definition

We idealize a composite wing as a flat rectangular composite plate fixed on one edge, free on all other edges, as shown in Fig. 1. The dimensions and material properties used in our subsequent examples are shown in Table 1. The effect of ply orientation uncertainty is included by adding an independent and identically distributed Gaussian error, with zero mean and standard deviation of five degrees, to each ply orientation.

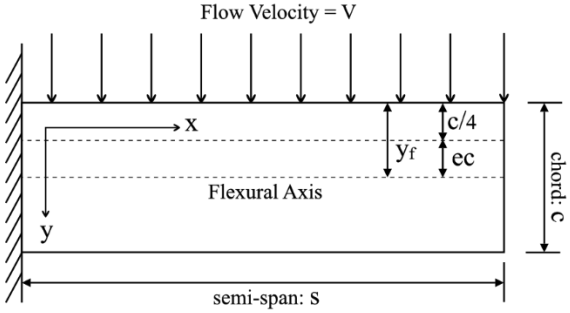

Figure 1. Composite Plate Geometry

Table 1. Dimensions and material properties used in examples

Semi-span (m)	Chord (m)	E_{11} (GPa)	E_{22} (GPa)	G_{12} (GPa)	υ_{12}	ρ (kg/m^3)	Ply Thickness (mm)
0.3048	0.0762	140	10	5	0.3	1600	0.125

III. Deterministic Aeroelastic Model

A. Composite Material Properties

In classical lamination theory[28], out-of-plane moment resultants are related to out-of-plane curvatures by

$$\boldsymbol{M} = \mathrm{D}\boldsymbol{\kappa} \tag{1}$$

where $\boldsymbol{M}$ and $\boldsymbol{\kappa}$ are the moment resultant and curvature vectors respectively. The out-of-plane laminate stiffness matrix, D, can be represented as a function of material invariants U_i (i = 1…5), laminate thickness t, and the out-of-plane lamination parameters ξ_i (i = 9…12) in accordance with

$$\begin{Bmatrix} D_{11} \\ D_{12} \\ D_{22} \\ D_{66} \\ D_{16} \\ D_{26} \end{Bmatrix} = \frac{t^3}{12} \begin{bmatrix} 1 & \xi_9 & \xi_{10} & 0 & 0 \\ 0 & 0 & -\xi_{10} & 1 & 0 \\ 1 & -\xi_9 & \xi_{10} & 0 & 0 \\ 0 & 0 & -\xi_{10} & 0 & 1 \\ 0 & \frac{\xi_{11}}{2} & \xi_{12} & 0 & 0 \\ 0 & -\frac{\xi_{11}}{2} & \xi_{12} & 0 & 0 \end{bmatrix} \begin{Bmatrix} U_1 \\ U_2 \\ U_3 \\ U_4 \\ U_5 \end{Bmatrix} \tag{2}$$

By defining a non-dimensional through-thickness coordinate, u, the out-of-plane lamination parameters are defined in terms of ply orientations $\theta(u)$ as

$$\{\xi_9, \xi_{10}, \xi_{11}, \xi_{12}\} = \frac{3}{2}\int_{-1}^{1}\{cos2\theta(u), cos4\theta(u), sin2\theta(u), sin4\theta(u)\}u^2 du \tag{3}$$

where

$$u = \frac{2z}{t} \tag{4}$$

B. Aeroelastic Stability

The aeroelastic response of the plate is approximated using the Rayleigh Ritz method coupled strip theory[29]. Polynomial shape functions are assumed for the out-of-plane displacement in order to approximate energy terms, which are in turn minimised. Strain energy of the plate is given by

$$U = \frac{1}{2}\iint \boldsymbol{\kappa}^T D\boldsymbol{\kappa}\, dxdy \tag{5}$$

where D is as defined in Eq. (2) and the curvature vector $\boldsymbol{\kappa}$ is given as

$$\boldsymbol{\kappa} = \left\{-\frac{\partial^2 w}{\partial x^2} \quad -\frac{\partial^2 w}{\partial y^2} \quad -2\frac{\partial^2 w}{\partial x \partial y}\right\}^T \tag{6}$$

where w is the out-of-plane displacement. Kinetic energy is given by

$$T = -\frac{1}{2}\rho t \iint \dot{w}^2 dxdy \tag{7}$$

where a dotted parameter denotes a derivative with respect to time. The applied load is determined using a modified unsteady strip theory. Lift and pitching moment are applied to infinitesimal strips at the quarter chord and integrated over the length of the plate. The loads applied to each strip are given by

$$dL = \frac{1}{2}\rho_a V^2 c a_w \left(\theta + \frac{\dot{w}}{V}\right) dx \tag{8}$$

$$dM = \frac{1}{2}\rho_a V^2 c^2 \left(e a_w \left(\theta + \frac{\dot{w}}{V}\right) + M_{\dot{\theta}} \frac{\dot{\theta} c}{4V}\right) dx \tag{9}$$

where ρ_a and V denote the air density and velocity, c the chord length, e the eccentricity between quarter chord and flexural axis as defined in Fig. 1, and a_w the effective lift curve slope. Elastic twist is denoted by θ, which is given as

the derivative of the out-of-plane displacement with respect to the chord-wise coordinate *y*. A simplified analysis is used whereby the unsteady aerodynamic derivative $M_{\dot{\theta}}$ is assumed to be constant with respect to frequency changes. Previous work has validated the use of this modified strip theory for high aspect ratio composite wings at low airspeeds through comparison with the standard Doublet Lattice based approach[30]. Work done by the applied load is given by

$$W = \int_0^s (-dL\delta w + dM\delta\theta)dx \tag{10}$$

Neglecting dissipative energy, Lagrange's Equation may be applied as

$$\frac{d}{dt}\left(\frac{\partial T}{\partial \dot{\boldsymbol{q}}}\right) - \frac{\partial T}{\partial \boldsymbol{q}} + \frac{\partial U}{\partial \boldsymbol{q}} = \frac{\partial(\delta W)}{\partial(\delta \boldsymbol{q})} \tag{11}$$

where $\boldsymbol{q}$ are the generalised displacements. Application of Eq. (11) gives the equation of motion as

$$A\ddot{\boldsymbol{q}} + \rho_a V B\dot{\boldsymbol{q}} + (\rho_a V^2 C + E)\boldsymbol{q} = \boldsymbol{0} \tag{12}$$

where A is the inertia matrix, B and C are the aerodynamic damping and stiffness matrices respectively, and E is the stiffness matrix. Eq. (12) is solved as an eigenvalue problem to assess the stability of the wing at different air-speeds. Instability occurs when the real part of one of the eigenvalues becomes positive; this instability is flutter if the imaginary part is non-zero and divergence otherwise.

C. Deterministic Aeroelastic Behavior

Aeroelastic stability is a complicated phenomenon involving the coupling of aerodynamic forces with the bending and torsion motions of the structure. Aeroelastic tailoring enables the resulting characteristics to change; different laminate stacking sequences result in distinct instability mechanisms, and such changes can be observed across the design space of lamination parameters. Plots of the lowest instability speed can be seen to form a piecewise-smooth and continuous surface, with clearly visible boundaries where the surface is either non-smooth or discontinuous. Fig. 2 displays contours of instability speed with respect to different lamination parameter planes, assuming a laminate thickness of 2mm.

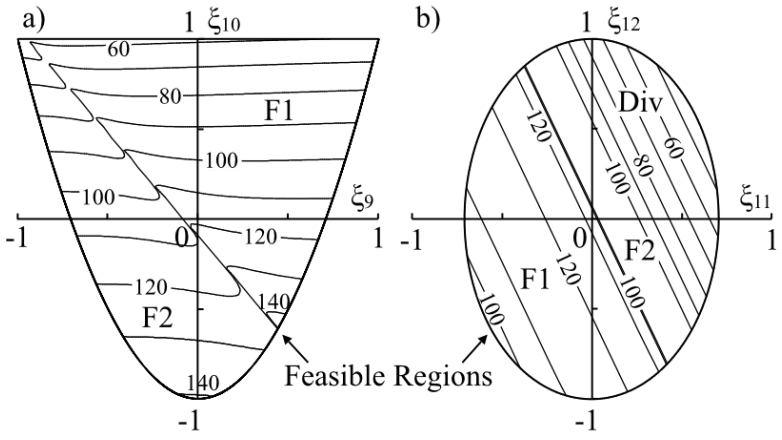

Figure. 2. Contours of Instability Speed (m/s) with Respect to the Lamination Parameters a) Uncoupled Parameter ($\xi_{9\text{-}10}$) Plane, $\xi_{11,\,12} = 0$ b) Bend-Twist Coupling Parameter ($\xi_{11\text{-}12}$) Plane, $\xi_{9,\,10} = 0$

Three types of behavior are evident in Fig. 2; divergence, and two flutter modes which are henceforth referred to as 'flutter 1' and 'flutter 2'. Through examination of the mode-shapes, flutter 1 can be attributed to coupling of the first bending and torsion vibration modes, and flutter 2 to coupling of the second bending and first torsion modes. Example eigenvalue plots for each instability mechanism are shown in Fig. 3.

An eigenvalue of the equation of motion is denoted by λ_j; in each of the cases in Fig. 3, at V = 0 m/s, λ_1 and λ_2 correspond to the 1st and 2nd bending modes and λ_3 to the 1st torsion mode, though the mode-shapes change considerably with increasing velocity. Of particular note is the cross-over of the imaginary parts of λ_2 and λ_3 which

occurs in Fig. 3b but not Fig 3a, due to the coalescence of the different eigenvalues with λ_1 in each case. Noting that a different eigenvalue becomes unstable for different types of flutter it is proposed that given a small variation in lamination parameters, such that the wind-off modes do not change in order, it is possible to separate different flutter types by considering the eigenvalues alone. Divergence may be distinguished from flutter as having eigenvalues with zero imaginary part, as shown in Fig. 3c.

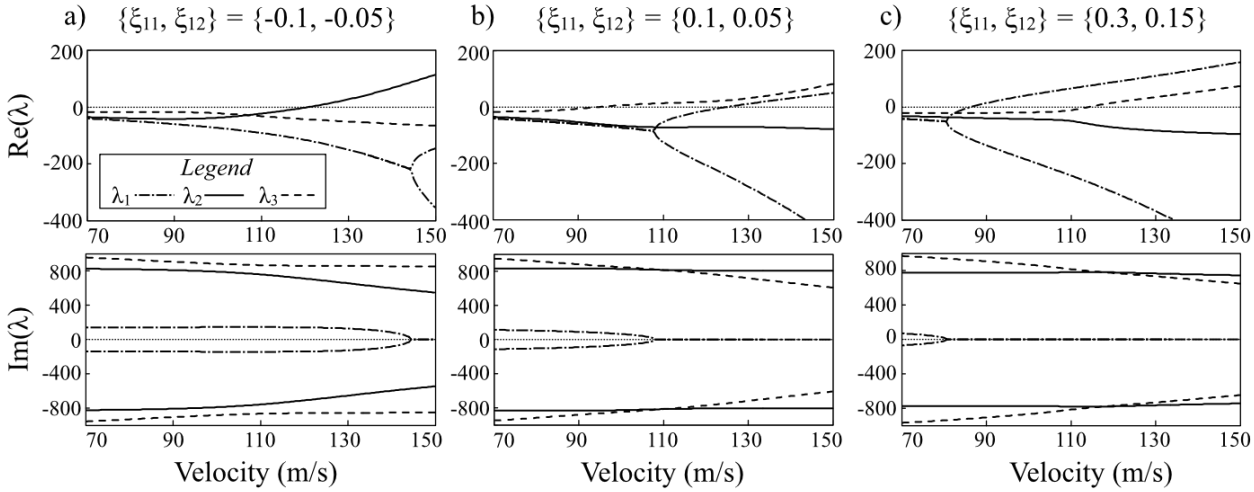

Figure 3. Eigenvalue plots for different instability Mechanisms: a) 'Flutter 1', b) 'Flutter 2', c) Divergence

IV. Stochastic Model

A. Stochastic Model Overview

Uncertainty quantification often requires a large number of runs of computationally expensive models, it can therefore be desirable to use an emulator which mimics behaviour of the model at reduced computational cost. We use Gaussian processes to emulate the aeroelastic model by fitting them to the aeroelastic instability speed at a small number of points selected using a maximin Latin Hypercube Design of Experiments. Probability Density Functions (PDFs) for instability speed are estimated by Monte Carlo Simulation (MCS) of the emulator.

In order to account for the discontinuities caused by the existence of different instability mechanisms, an emulator is fitted to each of the instability speeds, and the space of test points used for prediction in the Monte Carlo Simulation is partitioned according to the possible mechanisms. An overview of the process is illustrated in Fig. 4.

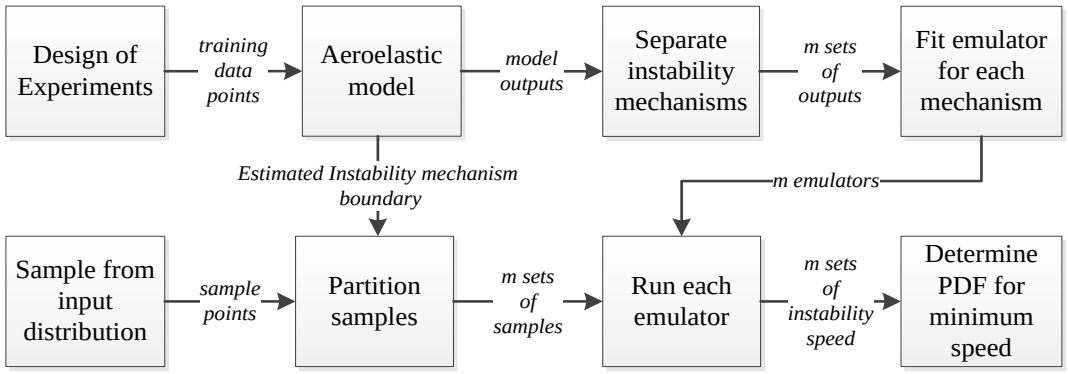

Figure 4. Uncertainty Quantification Overview

B. Gaussian Processes

A Gaussian process is a distribution over functions[18]. Rather than representing a function's output at each point with a deterministic value, a Gaussian process returns a Gaussian distribution. When used as an emulator this distribution represents the uncertainty associated with the emulator fit.

The model output y, can be considered a function of input vector $\boldsymbol{x}$, $y = f(\boldsymbol{x})$. If the value of $f(\boldsymbol{x})$ is known for a set of n training data points, $\{\boldsymbol{x}_1,\ldots,\boldsymbol{x}_n\}$, uncertainty about these data points can be represented as a multivariate Gaussian distribution. The mean of this distribution can be parameterised by basis functions $\boldsymbol{h}(\boldsymbol{x})^T$ as[20]

$$E\{f(\boldsymbol{x})|\boldsymbol{\beta}\} = \boldsymbol{h}(\boldsymbol{x})^T\boldsymbol{\beta} \tag{13}$$

conditional on the weight hyperparameter $\boldsymbol{\beta}$. For linear regression the basis vector, $\boldsymbol{h}(\boldsymbol{x})$, is taken as $(1, \boldsymbol{x}^T)$.

A fundamental assumption is that the output can be accurately represented by a smooth function, such that, if the value of $f(\boldsymbol{x})$ is known for point $\boldsymbol{x}$, this gives some indication of the value of $f(\boldsymbol{x}')$ for $\boldsymbol{x}'$ close to $\boldsymbol{x}$. This assumption is used in the covariance function

$$cov\{f(\boldsymbol{x}), f(\boldsymbol{x}')|\sigma^2, B\} = \sigma^2 c(\boldsymbol{x}, \boldsymbol{x}') \tag{14}$$

where

$$c(\boldsymbol{x}, \boldsymbol{x}') = exp\{-(\boldsymbol{x} - \boldsymbol{x}')^T B(\boldsymbol{x} - \boldsymbol{x}')\} \tag{15}$$

conditional on scaling factor σ^2 and roughness B, which is a diagonal matrix of length-scales. It can be seen that the covariance decreases as $|\boldsymbol{x} - \boldsymbol{x}'|$ increases, therefore points which are in close proximity are strongly correlated.

Eqs. (13-15) are combined in a Gaussian process prior distribution. Conditioning upon training data $\boldsymbol{y}$ at n data points yields the predictive distribution to be the Gaussian process[18]

$$[f(\boldsymbol{x})|\boldsymbol{y}, \sigma^2, B, \boldsymbol{\beta}] \sim GP\left(m^*(\boldsymbol{x}), c^*(\boldsymbol{x}, \boldsymbol{x}')\right) \tag{16}$$

where

$$m^*(\boldsymbol{x}) = \boldsymbol{\beta}^T[\boldsymbol{h}(\boldsymbol{x}) - H^T A^{-1}\boldsymbol{t}(\boldsymbol{x})] + \boldsymbol{y}^T A^{-1}\boldsymbol{t}(\boldsymbol{x}) \tag{17}$$

$$c^*(\boldsymbol{x}, \boldsymbol{x}') = c(\boldsymbol{x}, \boldsymbol{x}') - \boldsymbol{t}^T(\boldsymbol{x})A^{-1}\boldsymbol{t}(\boldsymbol{x}) \tag{18}$$

and

$$\boldsymbol{t}(\boldsymbol{x})^T = \{c(\boldsymbol{x}, \boldsymbol{x}_1), \ldots, c(\boldsymbol{x}, \boldsymbol{x}_n)\},\ H^T = \{\boldsymbol{h}^T(\boldsymbol{x}_1), \ldots, \boldsymbol{h}^T(\boldsymbol{x}_n)\},$$

$$A = \begin{pmatrix} 1 & c(\boldsymbol{x}_1, \boldsymbol{x}_2) & \ldots & c(\boldsymbol{x}_1, \boldsymbol{x}_n) \\ c(\boldsymbol{x}_2, \boldsymbol{x}_1) & 1 & & \vdots \\ \vdots & & \ddots & \\ c(\boldsymbol{x}_n, \boldsymbol{x}_1) & \ldots & & 1 \end{pmatrix} \tag{19}$$

noting that in Eqs. (16-19), $\boldsymbol{x}$ denotes a test-point for which the value of $f(\boldsymbol{x})$ is unknown and to be predicted, and $\{\boldsymbol{x}_1,\ldots\boldsymbol{x}_n\}$ are the training data points for which $\{f(\boldsymbol{x}_1),\ldots,f(\boldsymbol{x}_n)\}$ is known. It should be noted that Eq. 16 is conditional upon hyperparameters, σ^2, B, and $\boldsymbol{\beta}$. These parameters are assumed to take their most probable values, and are estimated using Maximum Likelihood Estimation (MLE)[18].

The output probability distribution can be estimated using Monte Carlo Simulation. For simplicity, the emulator mean, $m^*(\boldsymbol{x})$ in Eq. (17), is taken as a reasonable approximation for realisations of the Gaussian process in Eq. (16)[20].

C. Emulation of a Discontinuous Function

In order to satisfy the requirement of smoothness imposed by the choice of covariance function, a separate Gaussian process is fitted to the different instability mechanisms indicated in Fig. 2. Provided the variation in material properties is small, the different instability mechanisms may be distinguished on the basis of the eigenvalue which becomes unstable.

In order to accurately perform MCS with the multiple Gaussian processes, the test points are partitioned into regions. Inner boundaries of each of these regions are defined as a convex hull of the training data points for which the corresponding instability mechanism is possible, calculated using the '*convhulln*' function in MATLAB[31]. Points which lie outside of the convex hulls are grouped into the region whose centroid has minimal distance from the test point, weighted by the size of the hull. This process is illustrated in Fig. 5.

Once the test points are partitioned, the corresponding emulator mean is calculated for all points in each region, noting that there can be some overlap. The critical instability speed is approximated as the minimum emulator mean for each point.

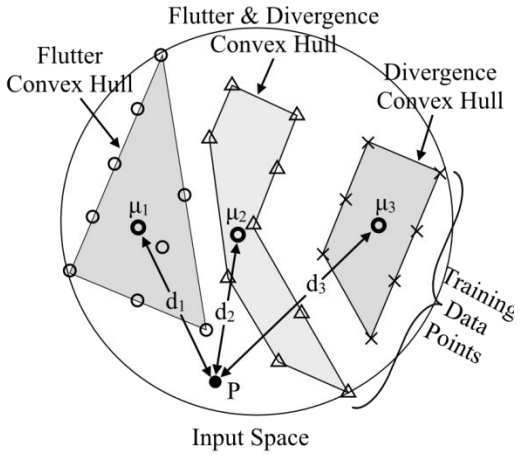

Figure 5. Partitioning the Test-points

D. Uncertainty Quantification Examples

In this section Probability Density Functions (PDFs) estimated using the approach described in Section C are compared with those determined using Monte Carlo Simulation of the plate model itself. A previous convergence study[12] has shown that MCS with 5000 samples gives sufficiently accurate PDFs for the critical instability speed.

For simple unimodal examples in which only one instability mechanism is possible, it is found that 30 training data points typically give sufficient accuracy. This result corresponds to an order of two magnitudes reduction in the number of model runs compared to Monte Carlo of the model itself. Fig. 6 compares an example PDF of a Gaussian process fitted with 30 training data points, to the PDF of the model itself, for a $[0_2\ 90_2]_{2S}$ laminate.

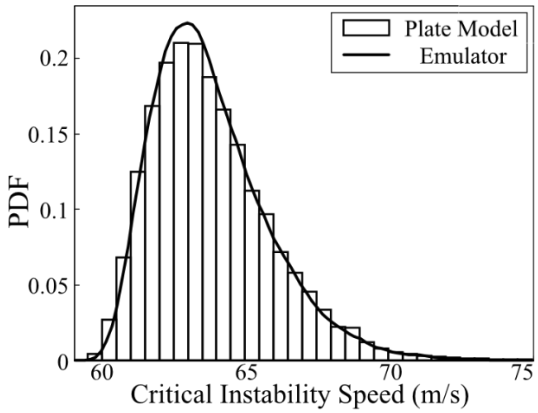

Figure 6. PDFs for a $[0_2\ 90_2]_{2S}$ Laminate

In order to demonstrate the ability to emulate the discontinuous behavior shown in Fig. 2, results for a $[45_2\ {-45_2}\ 0_2\ 90_2]_S$ and $[45\ {-45_3}\ 0_2\ 90_2]_S$ laminate are shown in Figs. 7-9.

Fig, 7a shows a surface plot of the critical aeroelastic instability speed with respect to bend-twist coupling parameters $\xi_{11\text{-}12}$, with $\xi_{9\text{-}10}$ set to their nominal values for the two examples. Two types of mode-switch can be observed; a switch from divergence to flutter at which point the instability speed is non-smooth, and a switch between two types of flutter where instability speed is discontinuous. Referring to Fig. 3, it is possible to see that instability speed is non-smooth at the divergence-flutter boundary since both divergence and flutter occur either side of the boundary, but occur in a different order with increasing velocity. The boundary between the two flutter modes is discontinuous since this requires the elimination of flutter 2, allowing flutter 1 to become critical.

The example laminates have been chosen such that uncertainty in their bend-twist coupling lamination parameters, $\xi_{11\text{-}12}$, cause these switches to occur. This effect is illustrated in Fig. 7b-c, which show enlarged details of contours for the critical instability speed overlaid with contours of the marginal PDF for $\xi_{11\text{-}12}$ for each examples. It can be seen that the PDF of the $[45_2\ {-45_2}\ 0_2\ 90_2]_S$ laminate in Fig. 7b crosses a divergence-flutter boundary, and the $[45\ {-45_3}\ 0_2\ 90_2]_S$ laminate PDF in Fig. 7c crosses a flutter-flutter boundary. Figs. 8 and 9 compare emulator PDFs with the PDF

of the plate model for these laminates. It can be seen that the non-smooth and discontinuous instability speed results in a bi-modal output PDF.

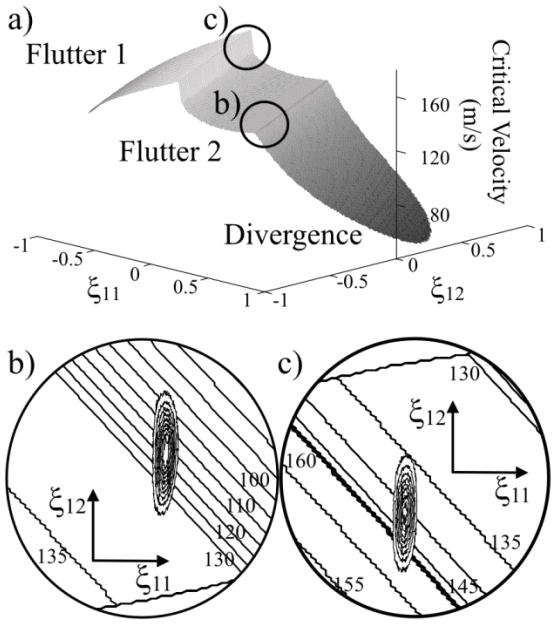

Figure 7. a) Surface of Critical Instability Speed with respect to ξ_{11-12}, with $\xi_9 = 0.094$, $\xi_{10} = -0.75$. Contour Details with ξ_{11-12} PDF overlaid for: b)$[45_2\ -45_2\ 0_2\ 90_2]_S$ and c) $[45\ -45_3\ 0_2\ 90_2]_S$

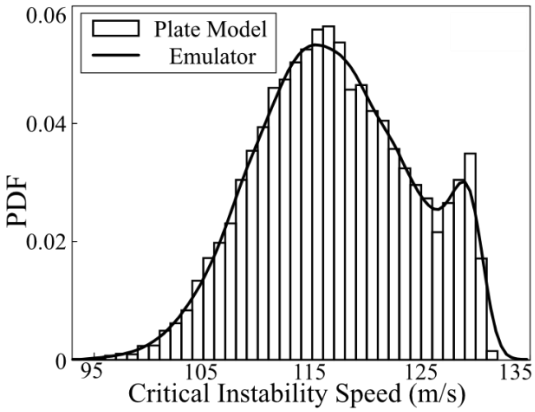

Figure 8. Output PDFs for a $[45_2\ -45_2\ 0_2\ 90_2]_S$ laminate

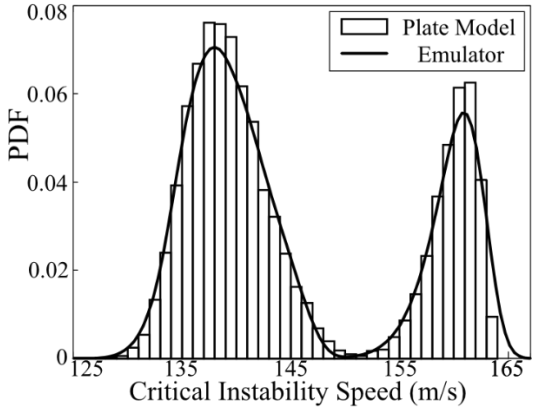

Figure 9. Output PDFs for a $[45\ -45_3\ 0_2\ 90_2]_S$ laminate

The emulator used in Fig. 8 was fitted using 30 training data points, which can be seen to provide a good fit to base-line Monte Carlo results, thereby offering the same order of two magnitudes reduction in model runs as in the uni-modal example. This is found to be typical of examples in the viscinity of a divergence-flutter boundary because training data points on either side of the boundary give information about both mechanisms. The emulator used in Fig. 9 required 100 training data points in order to provide a good fit, only offering an order of magnitude reduction in model runs compared to the baseline Monte Carlo. It was typically the case that extra training data was required in the vicinity of a boundary between flutter modes. We expect that this is in part due to the fact that information about flutter 2 is only available on one side of the boundary, and in part due to the inefficiency of the approach used to partition the test points.

V. Robust Optimization

A. Deterministic Optimization

A benchmark deterministic optimum is obtained in order to assess the quality of robust optimization results. Numerous approaches have been undertaken for optimizing composite structures[32]. Since the aeroelastic instability speed is discontinuous, local optima may exist. Furthermore, it is common when optimizing composites to fix ply orientations to a set of discrete values, therefore a genetic algorithm has been chosen as the most appropriate method.

The ply orientations are treated as the design variable. Two strategies are adopted, a first where orientations are fixed to 0°, 90°, and ±45°, and a second where ±30° and ±60° plies are also allowed. In this initial study instability speed is maximized. Although in practice it would be more useful to minimize weight and treat instability speed as a

constraint, having instability speed as an objective allows direct comparisons to be made with earlier parametric studies[12]. Laminates are assumed to be symmetric with 16 plies and a thickness of 2mm. The optimization is performed using the MATLAB global optimization toolbox[31].

Ply contiguity constraints are often applied to ensure no more than four plies of a given orientation are stacked together[33,34]. In order to maintain this constraint, a penalty function is added which counts the number of constraint violations.

B. Probabilistic Optimization

Numerous interpretations of robust design can be found in the literature. In this paper we adopt a strategy where the probability that aeroelastic instability occurs at design air speeds is minimised[27]. This strategy is equivalent to that which maximises the reliability of the structure[23]. The optimization problem can be stated as

$$\min_{y} P(V_{crit}(y) < V_{des}) \tag{20}$$

subject to the constraints discussed in the previous section. V_{des} denotes a design instability speed which is defined prior to the optimization.

The failure probability of a given design is estimated using Gaussian processes. An initial Latin Hypercube is generated with 30 training data points, and the plate model is run for each point. If a switch between flutter modes is detected a further 70 training data points are generated in order to ensure sufficient accuracy. The emulator is fitted as illustrated in Fig. 4 and the probability of failure is estimated using Monte Carlo Simulation of the emulator mean as

$$\mathrm{P}(V_{crit} < V_{des}) \approx \frac{1}{n}\sum_{i=1}^{n} I(m_i^*(\boldsymbol{x}_i) < V_{des}) \tag{21}$$

where $I(m^*_i(\boldsymbol{x}_i) < V_{des})$ is an indicator function which returns the values

$$I(m_i^*(\boldsymbol{x}_i) < V_{des}) = \begin{cases} 1, & m_i^* < V_{des} \\ 0, & otherwise \end{cases} \tag{22}$$

where $m^*_i(\boldsymbol{x}_i)$ is the predicted emulator mean for test point $\boldsymbol{x}_i$, given by Eq. 17. The estimated failure probabilities are equivalent to the area of the output PDF which lies below the design speed. As no design speed is specified for the deterministic optimization, as would be the case in a minimum weight design, several design speeds are considered so as to observe the effect upon the resulting robust optima.

C. Results

Deterministic and robust optima for the two layup strategies, and design speeds of 145m/s and 150m/s are shown in Table 2, along with the nominal value, mean and standard deviation of the instability speed, and probability of failure for the two design speeds. Figs. 10 and 11 compares the Probability Density Functions for the critical instability speed of the deterministic optima, as well as robust optima determined using two different design speeds.

Table 2. Optimization Results for 1) 0°, ±45° and 90° Plies and 2) 0°, ±30° ,±45°, ±60° and 90° Plies

Layup Strategy	Objective		Layup	V_{crit} (m/s)			Probability of Failure	
				Nom.	Mean	Std. Dev.	V_{des} = 145 m/s	V_{des} = 150 m/s
1	Deterministic		$[-45_2\ 45_2\ 0_2\ \mp45]_S$	164.5	153.4	9.3	0.28	0.38
	Robust	V_{des} = 145 m/s	$[-45_3\ 45_2\ -45_2\ 45]_S$	157.5	154.1	2.8	0.002	0.079
		V_{des} = 150 m/s	$[-45\ \pm45\ 0\ -45_2\ 0\ -45]_S$	158.5	155.5	3.7	0.022	0.054
2	Deterministic		$[-45_2\ 30\ -45\ 30_2\ 45\ 30]_S$	167.3	156.1	8.7	0.16	0.31
	Robust	V_{des} = 145 m/s	$[\mp45\ -30\ -45_3\ \mp30]_S$	159.0	156.3	3.1	0.0006	0.028
		V_{des} = 150 m/s	$[\mp45\ -30_2\ -45\ -30\ \pm45]_S$	161.0	158.4	3.8	0.002	0.022

The failure probabilities for each of the deterministic optima are notably high. For example, there is a 28% chance that the optimal laminate with 0°, ±45°, 90° plies would fail due to aeroelastic instability at 145 m/s. Referring to Figs. 2 and 7, it can be seen that the optimal instability speed is on the boundary between two flutter modes and therefore

at the edge of a discontinuity. When ply orientations are uncertain this results in bi-modal PDFs as shown in Figs. 10 and 11. The high probability of a switch to a flutter mode with lower instability speed, indicated by the lower peak of the PDFs, leads to a high probability of failure, illustrated by the area under this peak below the design speed.

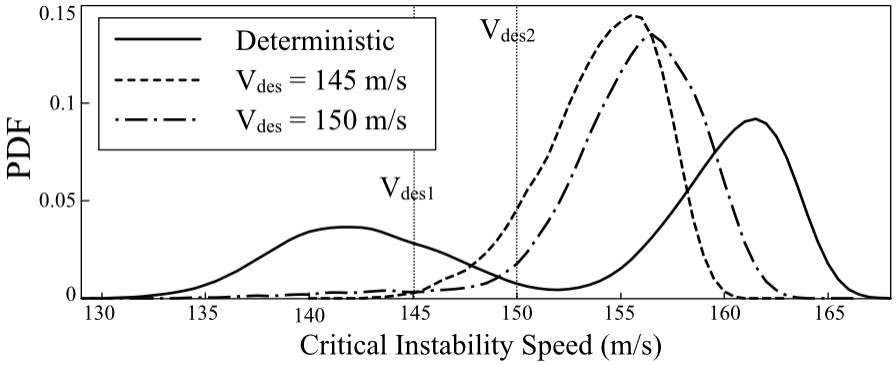

Figure 10. Comparison PDFs for different Optimial Laminates with 0°, ±45° and 90° Plies

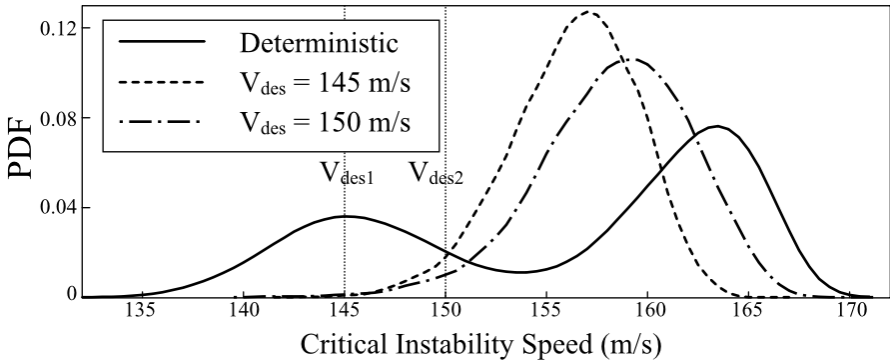

Figure 11. Comparison PDFs for different Optimial Laminates with 0°, ±30° ,±45°, ±60° and 90° Plies

With both layup strategies the robust optimization results in considerably more reliable designs, with significantly lower probabilities of failure. These lower failure probabilities are achieved by moving the design away from the discontinuity and therefore significantly reducing the size of the lower peak of the PDFs, or eliminating it completely. The probability of switching to a flutter mode with lower instability speed is therefore much recuced.

Using different design speeds in the objective function results in different optima. Figs. 2 and 7 show that the instability speed for flutter 1 decreases with increasing distance from the discontinuity. This causes the upper peak of the PDF to shift to the left, as can be seen in Fig. 10 for the 145 m/s robust design. A trade-off therefore exists in which the probability of a switching to a different mode must be lowered, without significantly increasing the probability of failure by the same flutter mode. In Fig. 10, the 145 m/s robust design has a relatively large area of the upper peak below 150 m/s and therefore a higher probability of failure at this speed. As such, the 150 m/s robust design is slightly closer to the discontinuity, thereby lowering the total area below the design speed despite a higher probability of a mode switch.

The long tails observed in Figs. 10 and 11 lower the mean instability speed relative to its nominal value for all of the optima. It is noteworthy that robust optimization results in both reduced variance and increased mean instability speed; this is atypical of robust design which is often considered to be a trade-off between mean performance and variance[25]. This improved averaged performance of the robust designs is thought to be due to the extent to which the mean instability speed of the deterministic optima is lowered by the bi-model behavior.

Finally, it can be remarked that there is a clear benefit to using ±30° and ±60° plies in the robust design. In the deterministic optimization, a 1.7% improvement in nominal instability speed is achieved over laminates with only 0°, ±45° and 90° plies. Much larger improvements to reliability are achieved by using ±30° and ±60° plies, the smallest being a 59% reduction in the probability of a failure of the 150 m/s robust design from 0.054 to 0.022. The PDFs in Fig. 11 are shifted to the right in comparison to those shown in Fig. 10. Therefore, it is thought that improvements in reliability are due to the extra available design space which gives access to higher instability speeds. This phenomenon is also thought to explain the lower failure probability of the deterministic optimum using the second layup strategy.

VI. Conclusions

An efficient approach has been presented for robust design of composite plate wings with uncertain ply orientations. Gaussian process emulators are used as surrogates for the aeroelastic instability speed in order to estimate the Probability Density Functions and failure probabilities at reduced computational cost. Probability of failure has been minimized using a genetic algorithm, and results have been compared to deterministic optima which maximize the instability speed. Two layup strategies were undertaken, a first which limits ply orientations to 0°, ±45°, and 90°, and a second which also uses ±30° and ±60° plies. The following observations have been made:

- The critical instability speed is discontinuous due to the existence of different instability mechanisms. This can result in bi-modal output Probability Density Functions when ply orientations are uncertain. The discontinuous behaviour can be efficiently approximated by fitting multiple emualtors to the different instability speeds.
- 30 training data points give sufficient accuracy for uncertainty quantification in the majority of examples, which corresponds to an order of two magnitudes reduction in model runs compared to MCS of the model itself.
- 100 training data points were required for sufficient accuracy in examples where a switch between flutter modes occurs, corresponding to an order of magnitude reduction in model runs.
- The benchmark deterministic optima have high probabilities of failure, as close proximity to the discontinuity between flutter modes means it is relatively probable that small variations will causes a switch to a flutter mode with lower instability speed.
- Through robust design a minimum improvement in reliability of 85.8% is achieved for laminates with 0°, ± 45° and 90° plies, and of 92.8% when ±30° and ±60° plies are introduced. The reliability is gained through moving designs away from the discontinuity thereby reducing the probability of a mode switch. This has the added benefit of increasing the average instability speed compared to the deterministic optima.
- Use of ±30°, ±60° plies in addition to 0°, ±45° and 90° plies results in a modest 1.7% improvement in nominal instabililty speed, but improvements in reliability of at least 59%.

It is noted, however, that the significantly larger number of training data points required to build the emulator in the region of a switch beween flutter modes limits the efficiency of the presented approach. It is anticipated that using classification techniques[35] or prior specification of the discontinuity in the emulator definition[36] could improve the efficiency. Efficiency is lost due to the need to recalculate Latin Hypercubes for each design, which prevents re-use of model outputs. It is proposed for future work that an active learning approach[37], whereby previously obtained results are retained and the same emulator is updated throughout the optimization process, could lead to substantial efficiency gains.

Acknowledgments

The authors would like to recognise the support of the EPSRC who fund the ACCIS Centre for Doctoral Training (EP/G036772/1), Embraer S.A, and also the Royal Academy of Engineering.

References

[1] Weisshaar, T. A., "Aeroelastic Tailoring of Forward Swept Composite Wings," *Journal of Aircraft*, Vol. 18, No. 8, 1981, pp. 669-676.

[2] Eastep, F.E., Tischler, V. A., Venkayya, V. B., Khot, N. S., "Aeroelastic Tailoring of Composite Structures," *Journal of Aircraft*, Vol. 36, No. 6, 1999, pp. 1041-1047.

[3] Weisshaar, T. A., Ryan, R. J., "Control of Aeroelastic Instabilities through Stiffness Cross-Coupling," *Journal of Aircraft*, Vol. 23, No. 2, 1986, pp. 148-155.

[4] Kameyama, M., Fukunaga, H., "Optimum Design of Composite Plate Wings for Aeroelastic Characteristics using Lamination Parameters," *Computers and Structures*, Vol. 85, No. 3-4, 2007, pp. 213-224.

[5] Pettit, C. L., Grandhi, R. V., "Optimization of a Wing Structure for Gust Response and Aileron Effectiveness," *Journal of Aircraft*, Vol. 40, No. 6, 2003, pp. 1185-1191.

[6] Kim, T. U., Hwang, I. H., "Optimal Design of a Composite Wing Subjected to Gust Loads," *Computers and Structures*, Vol. 83, No. 19-20, 2005, pp. 1546-1554.

[7] Pettit, C. L., "Uncertainty Quantification in Aeroelasticity: Recent Results and Research Challenges," *Journal of Aircraft*, Vol. 41, No. 5, 2004, pp. 1217-1229.

[8] Potter, K., Khan, B., Wisnom, M. R., Bell, T., Stevens, J., "Variability, Fibre Waviness and Misalignment in the Determination of the Properties of Composite Materials and Structures," *Composites: Part A*, Vol. 39, No. 9, 2008, pp. 1343-1354.

[9] Kahn, B., Potter, K., Wisnom, M. R., "Suppression of Delamination at Ply Drops in Tapered Composites by Ply Chamfering," *Journal of Composite Materials*, Vol. 40, No. 2, 2006, pp. 157-174.

[10] Liaw, D. G., Yang. H. T. Y., "Reliability of Uncertain Laminated Shells due to Buckling and Supersonic Flutter," *AIAA Journal*, Vol. 29, No. 10, 1993, pp. 1698-1708.

[11] Castravete, S. C., Ibrahim, R. A., "Effect of Stiffness Uncertainties on Flutter of a Cantilver Wing," *Journal of Aircraft*, Vol. 46, No. 4, 2008, pp. 925-935.
[12] Scarth, C., Cooper, J. E., Weaver, P. M., Silva, G. H. C., "Uncertainty Quantification of Aeroelastic Stability of Composite Plate Wings using Lamination Parameters," *Composite Structures*, Vol. 116, 2014, pp. 84-93.
[13] Bruno, L., Canuto, C., Fransos, D, "Stochastic Aerodynamics and Aeroelasticity of a Flat Plate via Generalized Polynomial Chaos", *Journal of Fluids and* Structures, Vol. 25, No. 7, 2009, pp. 1158-1176.
[14] Sarkar, S., Witteveen, J. A. S., Loeven, A., Bijl, H., "Effect of Uncertainty on the Bifurcation Behaviour of Pitching Airfoil Stall Flutter," *Journal of Fluids and Structures*, Vol. 25, No. 2, 2009, pp. 304-320.
[15] Xiu, D., Karniadakis, G. E., "The Wiener-Askey Polynomial Chaos for Stochastic Differential Equations," *SIAM Journal of Scientific Computing*, Vol. 24, No. 2, 2002, pp. 619-644.
[16] Babuska, I., Nobile, F., Tempone, R. A., "Stochastic Collocation Method for Elliptic Partial Differential Equations with Random Input Data," *SIAM Journal on Numerical Analysis*, Vol. 45, No. 3, 2006, pp. 1005-1034.
[17] Eldred, M. S., Burkardt, J., "Comparison of Non-Intrusive Polynomial Chaos and Stochastic Collocation Methods for Uncertainty Quantification," *47th AIAA Aerospace Sciences Meeting Including the New Horizons Forum and Aerospace Exposition*, AIAA, Orlando, Florida, 2009.
[18] Rasmussen, C. E., Williams, C. K. I, *Gaussian Processes for Machine Learning*, the MIT Press, 2006, ISBN 026218253X.
[19] Currin, C., Mitchell, T. J., Ylvisaker, D., "Bayesian Prediction of Deterministic Functions with Applications to the Design and Analysis of Computer Experiments," *Journal of the American Statistical Association*, Vol. 86, No. 416, 1991, pp. 953-963.
[20] Oakley, J. E., O'Hagan, A., "Bayesian Inference for the Uncertainty Distribution of Computer Model Outputs," *Biometrika*, Vol. 89, No. 4, 2002, pp. 769-784.
[21] Oakley, J. E., O'Hagan, A., "Probabilistic Sensitivity Analysis of Complex Models: a Bayesian Approach," *Journal of the Royal Statistical Society: Series B (Statistical Methodology)*, Vol. 66, No. 3, 2004, pp. 751-769.
[22] Choi, S. K, Grandhi, R. V., Canfield, R. A., *Reliability-based Structural Design*, Springer, London, 2007
[23] Allen, M., Maute, K., "Reliability-based Design Optimization of Aeroelastic Structures," *Structural and Multidisciplinary Optimisation*, Vol. 27, No. 4, 2004, pp. 228-242.
[24] Crespo, L. G., Giesy, D. P., Kenny, S. P., "Robustness Analysis and Robust Design of Uncertain Systems," *AIAA Journal*, Vol. 46, No. 2, 2008, pp. 388 – 396.
[25] Mourelatos, Z. P., Liang, J., "A Methodology for Trading-off Performance and Robustness under Uncertainty," *Journal of Mechanical Design*, Vol. 128, No. 4, 2005, pp. 856-863.
[26] Dodson, M., Parks, G. T., "Robust Aerodynamic Design Optimization using Polynomial Chaos," *Journal of Aircraft*, Vol. 46, No. 2, 2009, pp. 635-645.
[27] Manan, A., Cooper, J. E., "Design of Composite Wings Including Uncertainties: A Probabilistic Approach," *Journal of Aircraft*, Vol. 46, No. 2, 2009, pp. 601-607.
[28] Tsai, S. W., Hahn, H. T., *Introduction to Composite Materials*, Technomic Publishing Co., Inc., Lancaster, 1980.
[29] Wright, J. R., Cooper, J. E., *Introduction to Aircraft Aeroelasticity and Loads*, Wiley, New York, 2007.
[30] Stodieck, O., Cooper, J. E., Weaver, P. M., Kealy, P., "Improved aeroelastic tailoring using tow-steered composites," *Composite Structures*, Vol. 106, 2013, pp. 703-715.
[31] MATLAB, Software Package, Release 2012b, The MathWorks, Inc., Natick, Massachusetts, United States.
[32] Ghiasi, H., Pasini, D., Lessard, L., "Review: Optimum Stacking Sequence Design of Composite Materials Part 1: Constant Stiffness Design," *Composite Structures*, Vol. 90, 2009, pp. 1-11.
[33] Haftka, R. T., Walsh, J.L., "Stacking Sequence Optimization for Buckling of Laminated Plates by Integer Programming," *AIAA Journal*, Vol. 30, No. 3, 1992, pp. 814-819.
[34] Herencia, J. E., Weaver, P. M., Friswell, M. I., "Optimization of Long Anisotropic Laminated Fiber Composite Panels with T-shaped Stiffeners," *AIAA Journal*, Vol. 45, No. 10, 2007, pp. 2497-2509.
[35] Kotsiantis, S. B., "Supervised Machine Learning: A Review of Classification Techniques," *Informatica*, Vol. 31, 2007, pp. 249-268.
[36] Becker, W., Worden, K., Rowson, J., "Bayesian Sensitivity Analysis of Bifurcating Nonlinear Models," *Mechanical Systems and Signal Processing*, Vol. 34, No. 1-2, 2013, pp. 57-75.
[37] Echard, B., Gayton, N., Lemaire, M., "AK-MCS: An Active Learning Reliability Method Combining Kriging and Monte Carlo Simulation," *Structural Safety*, Vol. 33, 2011, pp. 145-154.